

# A Closely Spaced Dual-Band MIMO Patch Antenna with Reduced Mutual Coupling for 4G/5G Applications

Naser O. Parchin<sup>1, \*</sup>, Yasir I. A. Al-Yasir<sup>1</sup>,  
Haleh J. Basherlou<sup>2</sup>, and Raed A. Abd-Alhameed<sup>1</sup>

**Abstract**—This study proposes a low-profile dual-band MIMO patch antenna array with improved isolation for 4G-LTE and 5G wireless communications. The proposed antenna design contains two closely-spaced coaxial-fed patch antennas with U-shaped slots to generate dual-band operation at 2.6/3.6 GHz 4G/5G bands. The mutual coupling between MIMO elements can be reduced simultaneously at both operation bands by employing a pair of C-shaped parasitic structures with different sizes between the radiating patches. The results show that the isolation between the antenna ports has been enhanced by about 13 dB and 10 dB at the operation frequencies with the presence of the proposed parasitic structures. The simulation and measurements of the proposed antenna design have been provided to verify the performance of the design.

## 1. INTRODUCTION

Multiple-input-multiple-output (MIMO) systems with multiple-antenna units at both transmitter and receiver sides can take advantage of the multipath components sufficiently to enhance the performance of wireless systems [1–4]. The MIMO antenna arrays are widely used in the next generation of wireless communication systems. As MIMO technology can significantly enhance the capacity of the system and resist multipath fading, it has become a hot spot in the field of wireless communication [5–8].

In wireless systems, to maintain the independence of each antenna element in the MIMO system within a limited space, it is one of the urgent difficulties to overcome mutual coupling from the adjacent antenna, especially for dual-band arrays [8–10]. Mutual coupling is a phenomenon that depends upon the adjacent array elements and greatly affects the characteristics of wireless systems depending on array antennas and more recently MIMO wireless communication systems. To achieve low mutual coupling and high isolation between adjacent antenna elements and also suppressing the surface waves, several methods have been investigated [11–16]. The most common technique is to use the spatial diversity technique by separating antenna elements. However, this technique may not be suitable for most wireless systems, since it requires a relatively large space to place the antenna system. In order to improve the isolation of the planar antenna array, various decoupling methods such as defected ground slot (GDS) and parasitic structures have been introduced [17–20].

A compact design of a MIMO antenna utilizing a pair of C-shaped parasitic structures to reduce the mutual coupling of the dual-frequency/dual-port patch antennas is proposed. The configuration of the design is composed of two patch antenna elements fed by coaxial probes. By cutting a U-shaped slot on the radiation patch of the single-element design, the antenna can exhibit dual-frequency function. The results show that about 13 dB and 10 dB at mutual coupling reduction are achieved at first and second resonances, without any impact on the frequency bandwidth and radiation performance. The

---

*Received 30 January 2020, Accepted 9 April 2020, Scheduled 17 April 2020*

\* Corresponding author: Naser O. Parchin (n.ogaroudiparchin@bradford.ac.uk).

<sup>1</sup> Faculty of Engineering and Informatics, University of Bradford, Bradford, United Kingdom. <sup>2</sup> Bradford College, Bradford, United Kingdom.

antenna design is optimized to operate at 2.6 GHz/3.6 GHz. Thus, the proposed MIMO antenna can be used for fourth and fifth generation (4G/5G) wireless communications.

## 2. ANTENNA DESIGN AND CHARACTERISTICS

Figure 1(a) depicts the geometrical structure of the proposed dual-band patch antenna array. As can be observed, the antenna configuration contains two coaxial-fed rectangular patch antenna elements with U-shaped slots. In order to reduce the mutual coupling characteristic of the closely-spaced antenna elements, a pair of C-shaped parasitic structures have been embedded between the radiators. It is designed on an FR4 dielectric with characteristics of permittivity = 4.4, a thickness = 1.6 mm and a loss tangent = 0.02. The antenna is simulated using the CST software [21]. The parameter values of the designs are listed in Table 1. Fig. 1(b) illustrates the simulated  $S$ -parameter results. As illustrated, the design provides a good dual-band function with a reduced coupling at the resonance frequencies [22, 23].

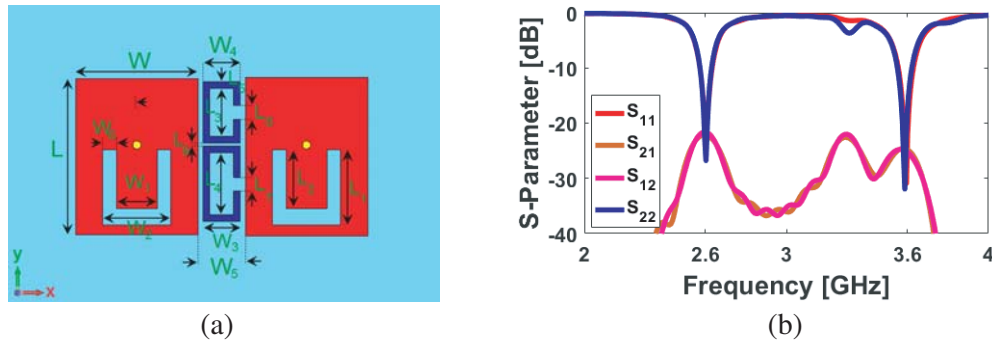


**Figure 1.** (a) Structure and (b) simulated  $S$ -parameters of the dual-band MIMO patch antenna.

**Table 1.** The values of the design parameters.

<b>Parameter</b>	$W$	$L$	$W_1$	$L_1$	$W_2$	$L_2$	$W_3$	$L_3$
<b>Value (mm)</b>	18	23	6	11	10	4.65	5.5	7
<b>Parameter</b>	$W_4$	$L_4$	$W_5$	$L_5$	$W_6$	$L_6$	$L_7$	$L_8$
<b>Value (mm)</b>	5.5	9	7	1	2	2	2	0.5

The simulated  $S_{11}$  results of the single patch antenna with and without the U-shaped slot are shown in Fig. 2(a). It is clearly observed that the basic patch antenna exhibits a single resonance operation while by employing the modified U-shaped slot, another resonance is achieved at the upper frequency [24, 25]. Therefore, a good dual-band function is generated for at 2.6/3.6 GHz 4G/5G applications. To have a better illumination about this dual-band operation, the simulated current densities at the resonance frequencies are depicted in Fig. 2(b). As seen, at the first resonance (2.6 GHz), most of the currents are mainly concentrated around the outer boundary of the rectangular radiation patch. In addition, at 3.6 GHz, the employed U-shaped slot is very active and highly surrounded by the currents verifying its role in creating the second resonance.

Figure 3(a) depicts the  $S_{21}$  characteristic of the design for various configurations. It can be observed that the design without the embedded parasitic structures provides  $-10$  dB and  $-18$  dB mutual coupling. By adding the first and second parasitic structures, the mutual coupling of the design is reduced at first and second resonance frequencies, respectively. The employed C-shaped parasitic structures act as a decoupling structure with band-pass filtering to reduce the mutual coupling of the MIMO antenna. Fig. 3(b) shows the simulated transmission/reflection characteristics ( $S_{11}/S_{21}$ ) of the single C-shaped parasitic structure. It shows a rejectband at the transmission zero frequency of 3.6 GHz. By using

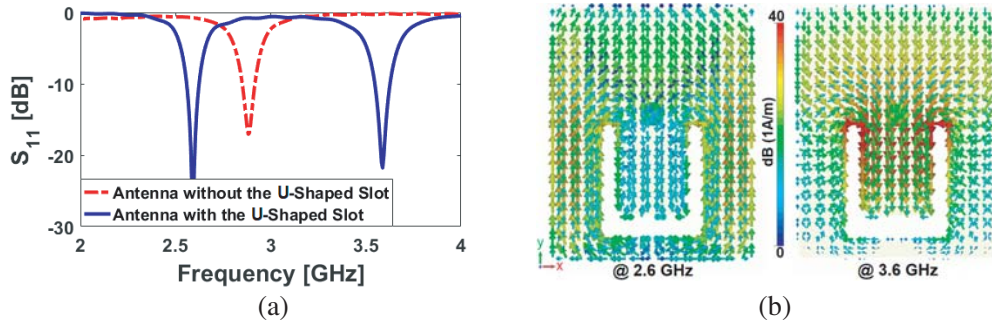


**Figure 2.** (a)  $S_{11}$  results for the antenna with and without the U-shaped slot and (b) current distributions at the resonance frequencies of the antenna element.

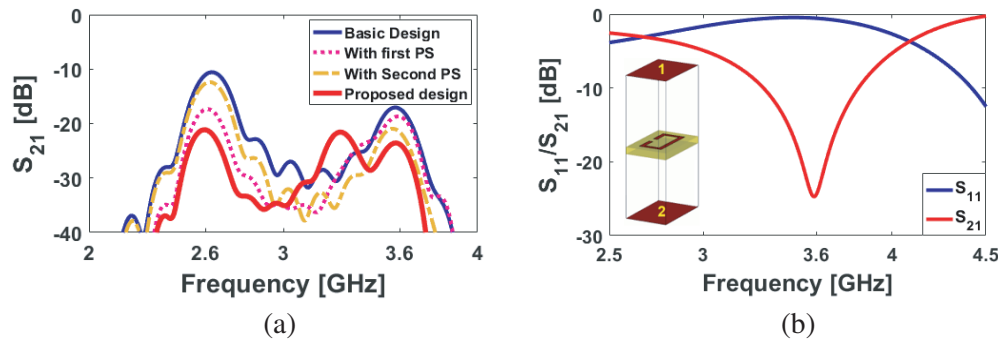


**Figure 3.** (a) Various mutual couplings of the design and (b)  $S$ -parameters of a C-shaped decoupling structure.

another C-shaped structure with optimizes dimension, a dual stop band response can be achieved to reduce the mutual coupling of the closely spaced dual-band MIMO antenna [26–28].

In order to have a better illumination about the working mechanism of the decoupling structures in the proposed design, the current distribution of the design without and with the parasitic structures at the resonance frequencies (2.6 GHz and 3.6 GHz) are studied and represented in Fig. 4. In this approach, the left antenna element is excited while the right one is terminated with a matched load of  $50 \Omega$ . It is observed from the figure that the mutual coupling has been significantly reduced with the implementation of the parasitic structures. In addition, the employed parasitic structures very active and highly surrounded by the currents at the relevant resonance frequencies [29–31]. As shown, the employed parasitic structures are very active at the relative frequencies and reduce the mutual function.

The reflection coefficient ( $S_{11}$ ) and transmission coefficient ( $S_{21}$ ) characteristics of the dual-band MIMO patch antenna array can be adjusted and tuned by changing the values for fundamental antenna parameters. The  $S_{11}/S_{22}$  results of the antenna mainly depend on the sizes of the antenna radiation patch and the U-shaped slot while the mutual coupling ( $S_{21}/S_{12}$ ) characteristic of the array can also be tuned by changing the parameters of the employed C-shaped parasitic structures [32–35]. In the following, the  $S_{11}$  and  $S_{21}$  results of the antenna for different values of the design parameters are investigated. Figs. 5 and 6 investigate the  $S_{11}$  and  $S_{21}$  characteristics of the proposed antenna for different values of the design parameters. Figs. 5(a)–(d) plot the  $S_{11}$  results for various values of  $L$  (length of the main radiator) and  $L_1$  (length of the U-slot),  $W_2$  (Width of U-slot), and,  $W$  (width of the radiation patch) respectively. As can be observed from Fig. 5(a), changing the length of the patch radiator has a significant impact on the first resonant frequency and just a little impact on the upper-frequency band. However, as shown in Fig. 5(b), the length of U-slot ( $L_1$ ) mainly affects the second resonance while it has a little impact on the first resonance at 2.6 GHz. Changing the value of  $W_2$  could affect both resonance frequencies as illustrated in Fig. 5(c). It can be also observed from 5(d) that unlike other parameters, changing the size of  $W$  does not affect the antenna frequency response significantly.

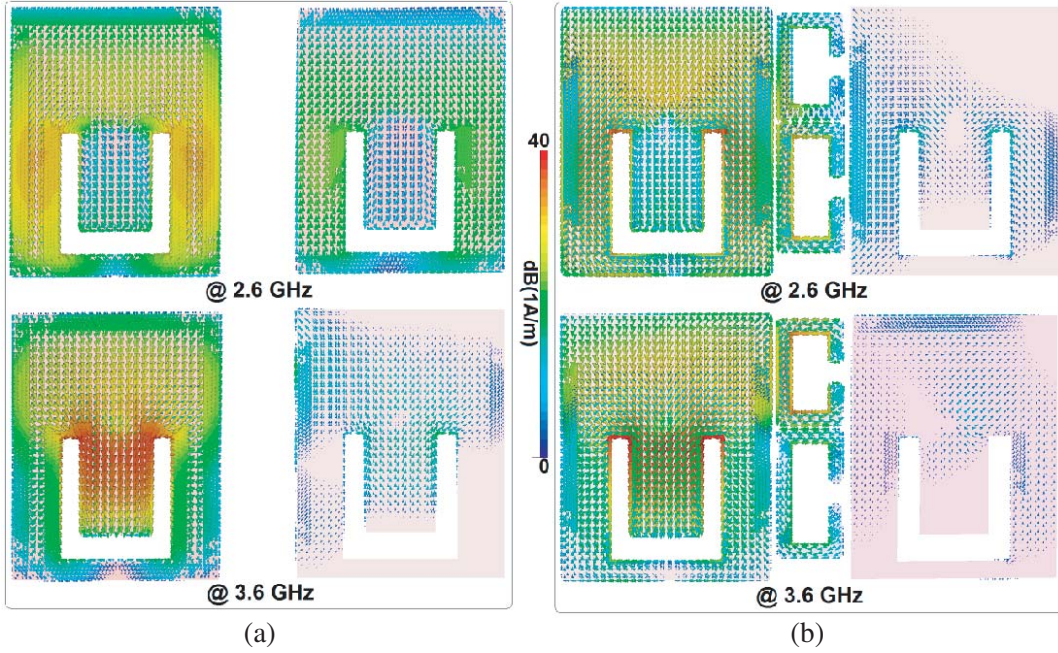


**Figure 4.** Current distributions at the resonance frequencies for the design (b) without and (c) with the employed parasitic structures.

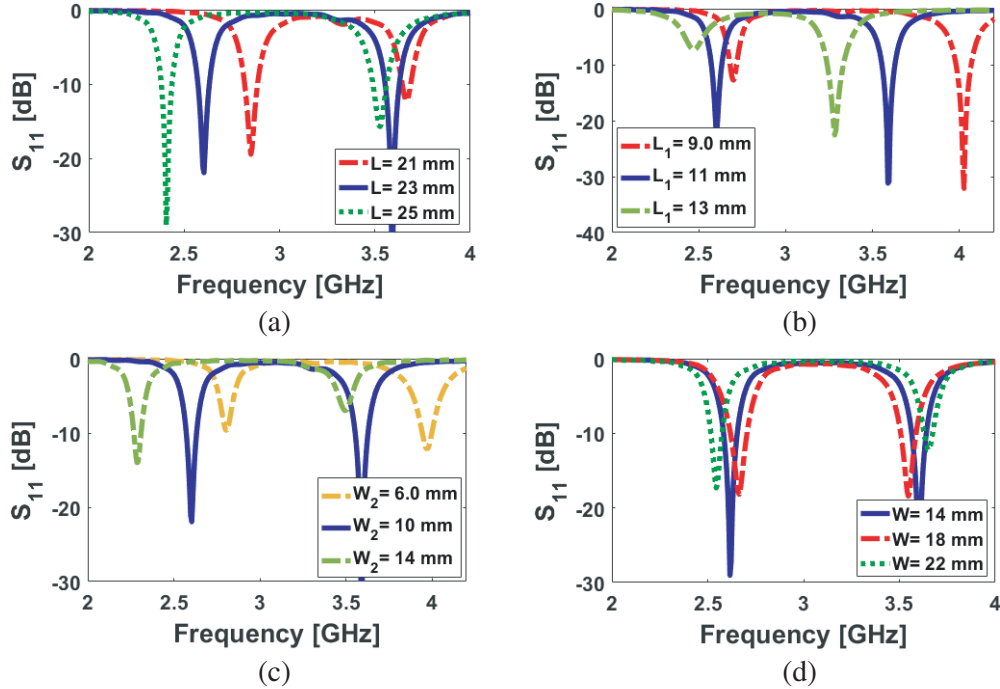


**Figure 5.**  $S_{11}$  characteristics for varying the values of (a)  $L$  and (b)  $L_1$ , (c)  $W$ , and (d)  $W_2$ .

Figures 6(a)–(d) illustrate the antenna mutual coupling for different sizes of  $W_3$ ,  $L_6$ ,  $W_4$ , and  $L_7$ , respectively. It is shown in Fig. 6(a) that by varying the width of the second parasitic structure ( $W_3$ ), the mutual coupling function at the first operation band (2.6 GHz) can be highly varied. As evident from Fig. 6(b), unlike  $W_3$ , changing the size of  $L_6$  has no impact on the mutual coupling if the array at 2.6 GHz. However, at 3.6 GHz, the mutual coupling characteristic is influenced and tuned significantly.

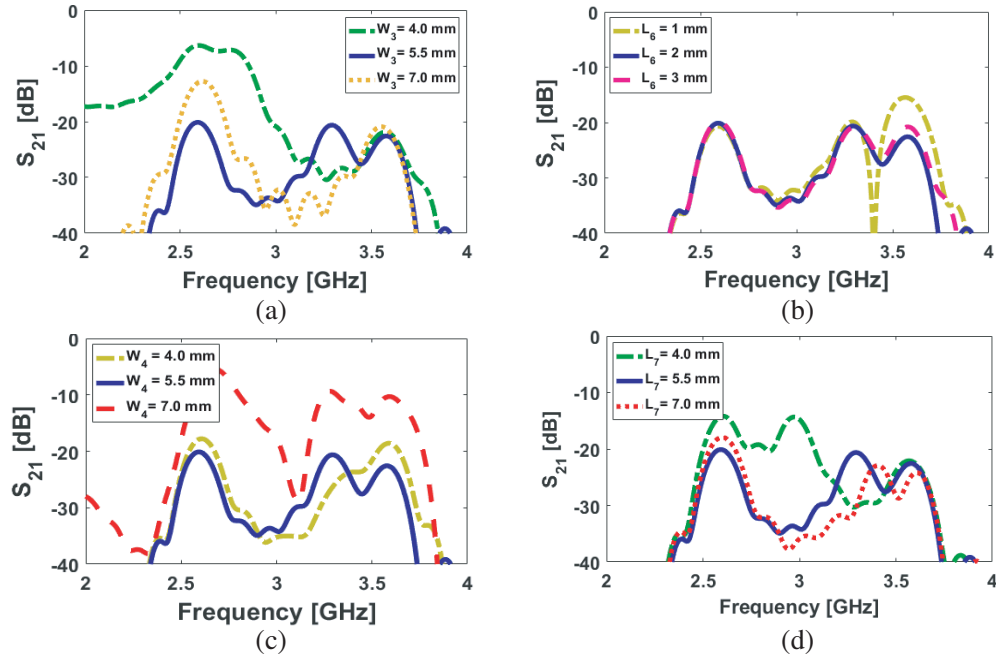


**Figure 6.**  $S_{21}$  (mutual coupling) characteristics for different values of (a)  $W_3$ , (b)  $L_6$ , (c)  $W_4$ , and (d)  $L_7$ .

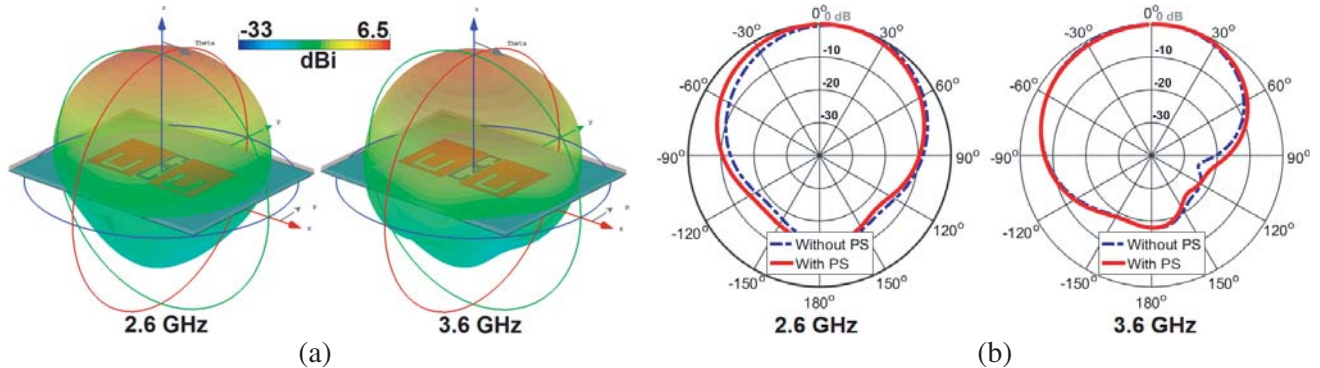


**Figure 7.** (a) 3D-radiation patterns of the antenna at 2.6/3.6 GHz with directivity values and (b) 2D-polar normalized patterns ( $H$ -plane) with/without parasitic structures at the resonance frequencies.

In addition, as shown in Fig. 6(c), changing the value of  $W_4$ , could affect the mutual coupling of the MIMO design at both resonance frequencies. However, unlike other parameters, changing the size of  $L_7$  does not affect the mutual coupling significantly. The 3D radiation patterns of the proposed MIMO antenna elements are illustrated in Fig. 7(a). It is evident that the MIMO design exhibit good radiation behaviour with high directivity characteristic. It can be also observed from Fig. 7(b) that the antenna exhibits good 2D-polar normalized patterns with low side and back lobes at the resonance frequencies [36–38].

The MIMO antenna has been fabricated on a cheap FR4 substrate and its  $S$ -parameters were measured to validate experimentally the approach to achieve good isolation and mutual coupling reduction. Fig. 8(a) illustrates the photograph of the fabricated antenna array. Fig. 8(b) compares the simulated and measured  $S$ -parameters of the proposed dual-band MIMO patch antenna array. It can be observed that the fabricated prototype exhibits good  $S$ -parameter results with an acceptable agreement with the simulated results.

The envelope correlation coefficient (ECC) and total active reflection coefficient (TARC)

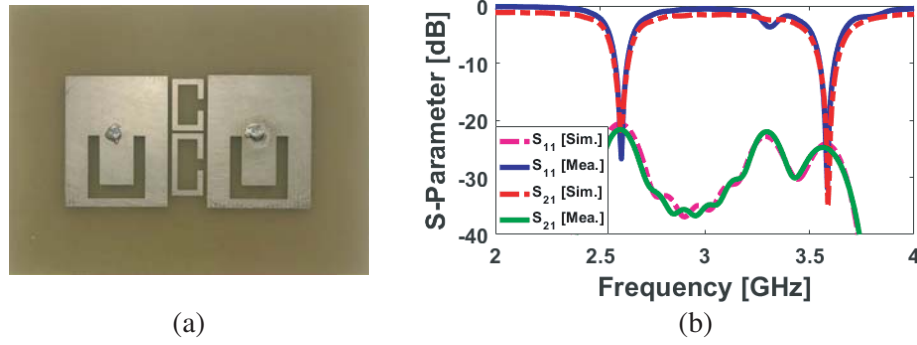


**Figure 8.** (a) The prototype sample and (b)  $S$ -parameters ( $S_{11}/S_{21}$ ) of the dual-band antenna.

characteristics are important parameters in diversity/MIMO antennas [39, 40]. The ECC and TARC characteristics of MIMO antenna can be calculated from  $S$ -parameter results using the below formulas:

$$\text{ECC} = \frac{|S_{mm}^* S_{mn} + S_{nm}^* S_{nn}|^2}{(1 - |S_{mm}|^2 - |S_{mn}|^2)(1 - |S_{nm}|^2 - |S_{nn}|^2)^*} \quad (1)$$

$$\text{TARC} = -\sqrt{\frac{(S_{mm} + S_{mn})^2 + (S_{nm} + S_{nn})^2}{2}} \quad (2)$$

Figure 9 represents the calculated ECC and TARC characteristics for the proposed dual-port diversity antenna. As shown in Figs. 9(a) and (b), the ECC and TARC results of this dual-band MIMO antenna are very low within the operation bands proving that the designed dual-band antenna is competent for diversity reception/transmission in the MIMO channels. Furthermore, it can be observed that the ECC and TARC results of the antenna are reduced by using the employed parasitic structure in the proposed antenna.

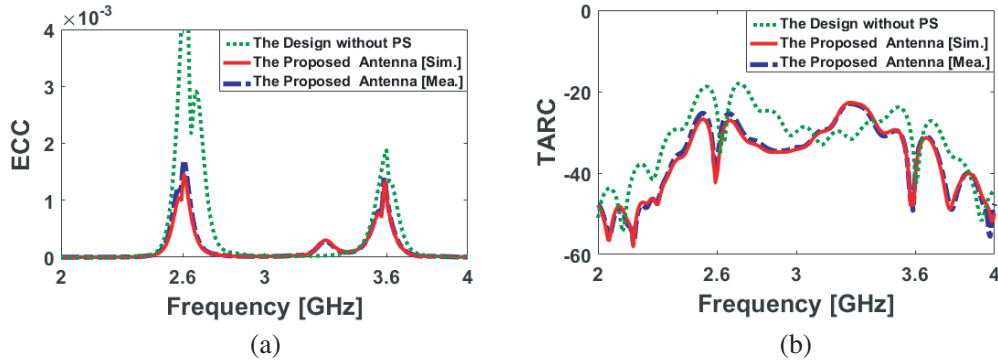


**Figure 9.** Calculated (a) ECC and (b) TARC results of the dual-band MIMO antenna w/o the parasitic structure (PS).

### 3. LINEAR ARRAY PERFORMANCE OF THE ANTENNA

The linear array performance of the designed dual-band patch antenna is studied in this section. Fig. 10(a) depicts the schematic of the linear array. As shown, it is composed of eight dual-band patch antennas with decoupling structures arranged in a linear form. The simulated  $S$ -parameters of the design are given in Fig. 10(b). It can be observed that the proposed phased array can exhibit good  $S$ -parameters at the target operation band. Moreover, the array provides low mutual coupling, less than  $-20$ , at the resonance frequencies. The main radiation beams of the array at 2.6 and 3.6 GHz are

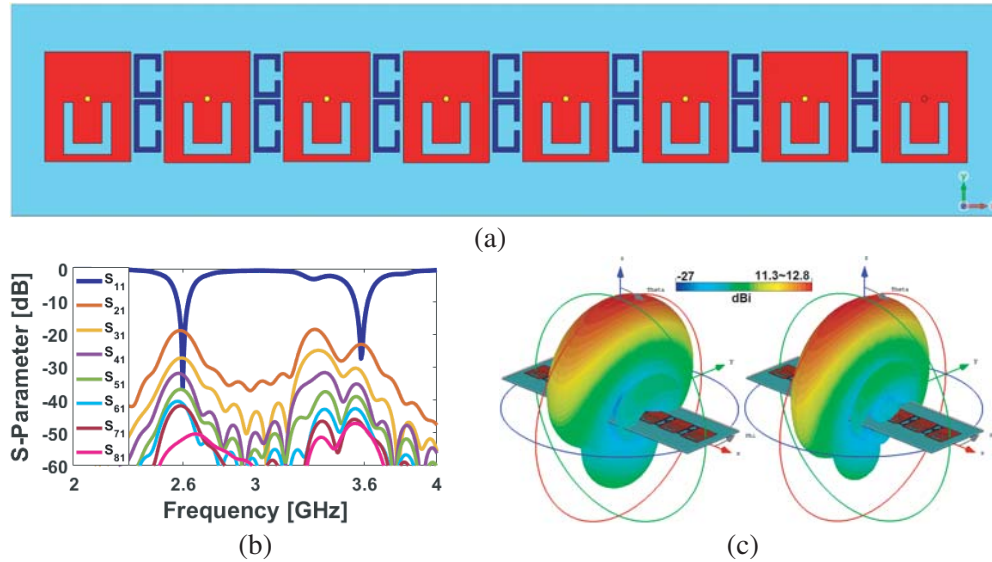


**Figure 10.** (a) Schematic, (b) *S*-parameters and (c) radiation beams of the linear antenna array at 2.6/3.6 GHz, respectively.

illustrated in Fig. 10(c). It is evident that the array has high-gain radiation beams with low side/back lobes which can be easily scanned to different angles [41, 42].

Figure 11 illustrates the directivity characteristics of the arrays (at 0° scanning angle) with different numbers of elements. As clearly shown, by increasing the number of antenna elements, the directivity values of the array at both 2.6 GHz and 3.6 GHz have been significantly increased, especially for 1 × 8 array design). In addition, the radiation beams of the array can be more directive which is sufficient for point to point communications [43–45].

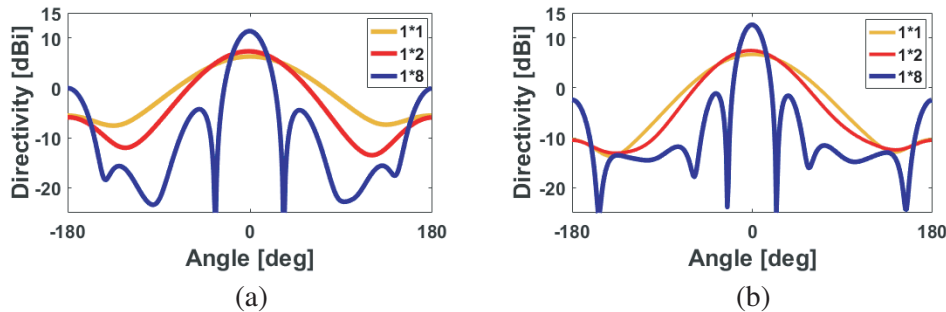


**Figure 11.** Directivities of the arrays with different numbers of the elements at (a) 2.6 GHz and (b) 3.6 GHz.

#### 4. CONCLUSION

In this paper, a new MIMO patch antenna array with a reduced mutual coupling function is proposed. The antenna configuration contains two coaxial-fed rectangular patch antenna elements with U-shaped slots. Simulations and measurements show that employing two C-shaped parasitic structures between the antenna elements effectively reduces the mutual coupling of the MIMO design at the desired operation bands simultaneously. The antenna is designed to work at 2.6 GHz and 3.6 GHz to support 4G and 5G frequency bands. Its linear array performance is also discussed. The proposed dual-band MIMO patch antenna has a planar and simple structure and can be easily integrated with the circuit boards.

## ACKNOWLEDGMENT

This work is supported by the European Union's Horizon 2020 research and innovation program under grant agreement H2020-MSCA-ITN-2016 SECRET-722424.

## REFERENCES

1. Yang, H. H. and Y. Q. S. Quel, "Massive MIMO meet small cell," *SpringerBriefs in Electrical and Computer Engineering*, 2017, DOI 10.1007/978-3-319-43715-6\_2.
2. Parchin, N. O., et al., "Microwave/RF components for 5G front-end systems," *Avid Science*, 1–200, 2019.
3. Balanis, C. A., *Antenna Theory*, 3rd Edition, Chapters 2, 4, 6, and 7, John Wiley, 2005.
4. Ojaroudi, N. and N. Ghadimi, "Dual-band CPW-fed slot antenna for LTE and WiBro applications," *Microw. Opt. Technol. Lett.*, Vol. 56, 1013–1015, 2014.
5. Hussain, R., A. T. Alreshaid, S. K. Podilchak, and M. S. Sharawi, "Compact 4G MIMO antenna integrated with a 5G array for current and future mobile handsets," *IET Microw. Antennas Propag.*, Vol. 11, 271–279, 2017.
6. Ojaroudi, Y., et al., "Circularly polarized microstrip slot antenna with a pair of spur-shaped slits for WLAN applications," *Microw. Opt. Technol. Lett.*, Vol. 57, 756–759, 2015.
7. Abdulkhaleq, A. M., et al., "Mutual coupling effect on three-way doherty amplifier for green compact mobile communications," *EuCAP 2020*, Copenhagen, Denmark, 2020.
8. Ojaroudi, N. and N. Ghadimi, "Design of CPW-fed slot antenna for MIMO system applications," *Microw. Opt. Technol. Lett.*, Vol. 56, 1278–1281, 2014.
9. Ojaroudiparchin, N., et al., "Multi-layer 5G mobile phone antenna for multi-user MIMO communications," *Proc. 23rd Telecommun. Forum Telfor (TELFOR)*, 559–562, Nov. 2015.
10. Kim, S. and S. Nam, "A compact and wideband linear array antenna with low mutual coupling," *IEEE Trans. Antennas Propag.*, Vol. 67, 5695–5699, 2019.
11. Parchin, N. O., et al., "Eight-element dual-polarized MIMO slot antenna system for 5G smartphone applications," *IEEE Access*, Vol. 9, 15612–15622, 2019.
12. Rajo-Iglesias, E., Ó. Quevedo-Teruel, and L. Inclán-Sánchez, "Mutual coupling reduction in patch antenna arrays by using a planar EBG structure and a multilayer dielectric substrate," *IEEE Transactions on Antennas and Propagation*, Vol. 56, 1648–1655, 2008.
13. Malmstrom, J., H. Holter, and B. L. G. Jonsson, "On mutual coupling and coupling paths between antennas using the reaction theorem," *IEEE Trans. Electromagn. Compat.*, Vol. 60, 2037–2040, 2018.
14. Alzahed, A. M., S. M. Mikki, and Y. M. M. Antar, "Nonlinear mutual coupling compensation operator design using a novel electromagnetic machine learning paradigm," *IEEE Antennas Wireless Propag. Lett.*, Vol. 18, 861–865, 2019.
15. Nurhayati, G. Hendrantoro, F. Takeshi, and E. Setijadi, "Mutual coupling reduction for a UWB coplanar vivaldi array by a truncated and corrugated slot," *IEEE Antennas and Wireless Propagation Letter*, Vol. 17, 2018.
16. Iqbal, A., O. A. Saraereh, A. W. Ahmad, and S. Bashir, "Mutual coupling reduction using F-shaped stubs in UWB-MIMO antenna," *IEEE Access*, Vol. 6, 2755–2799, 2018.
17. Hameed, K. W. H., et al., "The performance of SLNR beamformers in multi-user MIMO systems," *Broad Nets' 2018*, Faro, Portugal, 2018.
18. Kiani-Kharaji, M., H. R. Hassani, and S. Mohammad-Ali-Nezhad, "Wide scan phased array patch antenna with mutual coupling reduction," *IET Microw., Antennas Propag.*, Vol. 12, 1932–1938, 2018.
19. Mazloum, J., et al., "Compact triple-band S-shaped monopole diversity antenna for MIMO applications" *Applied Computational Electromagnetics Society (ACES) Journal*, Vol. 28, 975–980, 2015.

20. Basherlou, H. J., et al., "MIMO monopole antenna design with improved isolation for 5G WiFi applications," *International Journal of Electrical and Electronic Science*, Vol. 7, 1–5, 2019.
21. *CST Microwave Studio*, ver. 2018, CST, Framingham, MA, USA, 2018.
22. Ojaroudi, N., "Design of microstrip antenna for 2.4/5.8 GHz RFID applications," *German Microwave Conference*, GeMic 2014, RWTH Aachen University, Germany, March 10–12, 2014.
23. Wong, K.-L., "Isolation between GSM/DCS and WLAN antennas in a PDA phone," *Microw. Opt. Technol. Lett.*, Vol. 45, 347–352, 2005.
24. Ojaroudi, N., et al., "Quad-band planar inverted-f antenna (PIFA) for wireless communication systems," *Progress In Electromagnetics Research Letters*, Vol. 45, 51–56, 2014.
25. Ojaroudi, N., et al., "A new design of triple-band WLAN/WiMAX monopole antenna for multiple-input/multiple-output applications," *Microwave and Optical Technology Letters*, Vol. 56, 2667–2671, 2014.
26. Parchin, N. O., et al., "Multi-band MIMO antenna design with user-impact investigation for 4G and 5G mobile terminals," *Sensors*, Vol. 19, 1–16, 2019.
27. Al-Yasir, Y., et al., "Design of very compact combline band-pass filter for 5G applications," *LAPC'2018*, UK, 2018.
28. Ojaroudi, N., et al., "Enhanced bandwidth of small square monopole antenna by using inverted U-shaped slot and conductor-backed plane," *Applied Computational Electromagnetics Society (ACES) Journal*, Vol. 27, 685–690, 2012.
29. Jiang, W., B. Liu, Y. Cui, and W. Hu, "High-isolation eight-Element MIMO array for 5G smartphone applications," *IEEE Access*, Vol. 7, 34104–34112, 2019.
30. Parchin, N. O., "Low-profile air-filled antenna for next generation wireless systems," *Wireless Personal Communications*, Vol. 97, 3293–3300, 2018.
31. Ojaroudi Parchin, N., et al., "Dual-polarized MIMO antenna array design using miniaturized self-complementary structures for 5G smartphone applications," *13th European Conference on Antennas and Propagation (EuCAP)*, Krakow, Poland, Mar. 31–Apr. 5, 2019.
32. Ojaroudi, M., et al., "Dual band-notch small square monopole antenna with enhanced bandwidth characteristics for UWB applications," *ACES J.*, Vol. 25, 420–426, 2012.
33. Ojaroudi, N., "Circular microstrip antenna with dual band-stop performance for ultra-wideband systems," *Microw. Opt. Technol. Lett.*, Vol. 56, 2095–2098, 2014.
34. Strytsin, I., S. Zhang, and G. F. Pedersen, "Performance investigation of a mobile terminal phased array with user effects at 3.5 GHz for LTE advanced," *IEEE Antennas and Wireless Propagation Letters*, Vol. 16, 1847–1850, 2017.
35. Ojaroudiparchin, N., et al., "Design of Vivaldi antenna array with end-fire beam steering function for 5G mobile terminals," *23rd Telecommunications Forum Telfor (TELFOR)*, 587–590, Belgrade, Serbia, Nov. 24–26, 2015.
36. Ojaroudi, N., et al., "Enhanced bandwidth of small square monopole antenna by using inverted Ushaped slot and conductor-backed plane," *Applied Computational Electromagnetics Society (ACES) Journal*, Vol. 27, 685–690, 2012.
37. Parchin, N. O., et al., "Dual-band monopole antenna for RFID applications," *Future Internet*, Vol. 11, 1–10, 2019.
38. Valizade, A., et al., "Band-notch slot antenna with enhanced bandwidth by using  $\Omega$ -shaped strips protruded inside rectangular slots for UWB applications," *Appl. Comput. Electromagn. Soc. (ACES) J.*, Vol. 27, 816–822, 2012.
39. Parchin, N. O., et al., "8  $\times$  8 MIMO antenna system with coupled-fed elements for 5G handsets," *IET Conference on Antennas and Propagation*, Birmingham, UK, Nov. 2019.
40. Parchin, N. O. and R. A. Abd-Alhameed, "A compact Vivaldi antenna array for 5G channel sounding applications," *EuCAP*, London, UK, 2018.
41. Parchin, N. O., et al., "A radiation-beam switchable antenna array for 5G smartphones," *2019 Photonics & Electromagnetics Research Symposium — Fall (PIERS — FALL)*, Xiamen, China, Dec. 17–20, 2019.

42. Parchin, N. O., et al., "MM-wave phased array quasi-yagi antenna for the upcoming 5G cellular communications," *Applied Sciences*, Vol. 9, 1–14, 2019.
43. Musavand, A., et al., "A compact UWB slot antenna with reconfigurable band-notched function for multimode applications," *Applied Computational Electromagnetics Society (ACES) Journal*, Vol. 13, No. 1, 975–980, 2016.
44. Ullah, A., et al., "Coplanar waveguide antenna with defected ground structure for 5G Millimeter wave communications," *IEEE MENACOMM'19*, Bahrain, 2019.
45. Ojaroudiparchin, N., et al., "Small-size tapered slot antenna (TSA) design for use in 5G phased array applications," *Applied Computational Electromagnetics Society Journal*, Vol. 32, 193–202, 2018.